# Third-order structure function in the logarithmic layer of boundary-layer turbulence

Jin-Han Xie, Charitha de Silva, Rio Baidya, Xiang IA Yang, and Ruifeng Hu

Phys. Rev. Fluids **6**, 074602 — Published 6 July 2021

DOI: 10.1103/PhysRevFluids.6.074602

# On the third-order structure function in the logarithmic layer of boundary-layer turbulence

Jin-Han Xie[1a], Charitha de Silva[2], Rio Baidya[3], Xiang IA Yang[4b], and Ruifeng Hu[5c]
[1]Department of Mechanics and Engineering Science, College of Engineering and LTCS, Peking University, Beijing 100871, PR China
[2]School of Mechanical and Manufacturing Engineering, University of New South Wales, Sydney, 2052, Australia
[3]Institution of Fluid Mechanics and Aerodynamics, Bundeswehr University Munich, Neubiberg, 85579, Germany
[4]Mechanical Engineering, Pennsylvania State University, State College, PA, 16802, USA
[5]Center for Particle-Laden Turbulence, Key Laboratory of Mechanics on Disaster and Environment in Western China, Ministry of Education, and College of Civil Engineering and Mechanics, Lanzhou University, Lanzhou 730000, PR China

Townsend's attached eddy hypothesis (AEH) gives an accurate phenomenological description of the flow kinematics in the logarithmic layer, but it suffers from two major weaknesses. First, AEH does not predict the constants in its velocity scalings; and second, none of the predicted velocity scalings can be obtained from the Navier-Stokes (NS) equations under AEH's assumptions. These two weaknesses separate AEH from more credible theories like Kolmogorov's theory of homogeneous isotropic turbulence, which, despite its phenomenological nature, has one velocity scaling, i.e., $\langle \Delta u^3 \rangle = -(4/5)\epsilon r$, that can be derived from the NS equation. Here, $\langle \Delta u^3 \rangle$ is the longitudinal third-order structure function, $\epsilon$ is the time-averaged dissipation rate, and $r$ is the displacement between the two measured points. This work aims to address these two weaknesses by investigating the behavior of the third-order structure function in the logarithmic layer of boundary-layer turbulence. We invoke AEH and obtain $\langle \Delta u^3 \rangle = D_3 \ln(r/z) + B_3$, where $\Delta u$ is the streamwise velocity difference between two points that are displaced by a distance $r$ in the streamwise direction, $z$ is the wall-normal location of the two points, $D_3$ is a universal constant, and $B_3$ is a constant. We then evaluate the terms in the Kármán-Howarth-Monin (KHM) equation according to AEH and see if NS equations give rise to a non-trivial result that is consistent with AEH. Last, by resorting to asymptotic matching, we determine $D_3 = 2.0$ (at sufficiently high Reynolds numbers).

## I. INTRODUCTION

Boundary-layer turbulent flows are ubiquitous and essential for numerous engineering applications and natural phenomena. In the vicinity of a solid boundary, there is a layer where the production and dissipation of turbulence kinetic energy approximately balance [1–4]. This layer is known as the logarithmic layer and is the focal point of many modeling works [5, 6]. For example, in his early work, Townsend [2] hypothesized that the flow in the logarithmic layer could be modeled as a collection of wall-attached eddies. Townsend's attached eddy hypothesis (AEH) provides an accurate phenomenological description of the flow kinematics in the logarithmic layer [7–11], and it gives accurate predictions of velocity scalings in the logarithmic layer [12–15]. However, AEH suffers from two major weaknesses. First, AEH does not predict the constants in velocity scalings. For example, AEH predicts the second-order structure function as the following expression, i.e., $\langle \Delta u^2 \rangle = 2A_1 \ln(r/z) + B_2$, but the Townsend-Perry constant $A_1$ is undetermined (let alone the flow-dependent constant $B_2$). Here, $\Delta u$ is the streamwise velocity difference between two points in the logarithmic layer that are displaced by a distance $r$ in the streamwise direction, $z$ is the wall-normal location of the two points. Here and throughout the paper, velocity normalization by the friction velocity $u_\tau$ is implied. The second weakness of AEH is that the predicted velocity scalings cannot be obtained from the Navier-Stokes (NS) equations. For example, the correctness of $\langle \Delta u^2 \rangle = 2A_1 \ln(r/z) + B_2$ relies solely on empirical data [16, 17].

[a] jinhanxie@pku.edu.cn
[b] xzy48@psu.edu
[c] hurf@lzu.edu.cn

Davidson et al. [18, 19] proposed to address the first weakness, i.e., the prediction of the constants in the velocity scalings, by giving up on AEH altogether. The authors pointed out that AEH is only one of the many possible rationalizations of the experimental data. They argued that rather than hypothesizing about the spatial organization of the eddies, it would be more fruitful to hypothesize about the energy density $E$ of $l$-sized eddies in the logarithmic layer. The authors proceeded by hypothesizing $E(l) \sim u_\tau^2/l$ for $l$ in the logarithmic layer. By matching the hypothesized log-layer energy density to that in the inertial range, the authors were able to get $\langle \Delta u^2 \rangle = 2A_1 \ln(r/z) + B_2$ and, more importantly, a prediction of the Townsend-Perry constant $A_1 = 1.81$ (the measured value is, however, $A_1 = 1.25$). Although Davidson and company did not explicitly resort to AEH, the hypothesized energy density $E(l) \sim u_\tau^2/l$ is consistent with AEH: according to AEH, $E(l)$ scales as $u_\tau^2 P(l)$ [2]; it then follows that $E(l) \sim u_\tau^2/l$ because $P(l) \sim 1/l$ is the eddy population density.

Addressing the second weakness requires the derivation of a known velocity scaling from the NS equation under the basic assumptions of AEH. This is non-trivial, and there is not too much literature on the topic. Marginally relevant studies are those that try to connect the basic assumptions of AEH to the NS equations. For example, Klewicki et al. [20, 21] analyzed numerical solutions to the NS equations and showed the presence of self-similar flow structures; Del Álamo and Jiménez [22], Sharma and McKeon [23], Moarref et al. [24], McKeon [25, 26], and Hwang and Eckhardt [27] showed that the (linearized/partly linearized) NS equations admit self-similar modes; Lozano-Duran and Bae [28] analyzed the length and velocity scales in the logarithmic layer and showed that they are consistent with AEH; Cheng et al. [29] identified attached eddies in low Reynolds number flows. The fact that one cannot obtain any AEH's velocity scaling from the Navier-Stokes equations separates AEH from the more credible theories like Kolmogorov's theory of small-scale turbulence. Despite its phenomenological nature, Kolmogorov's theory of small-scale turbulence has a velocity scaling in the inertial range, i.e.,

$$\langle \Delta u^3 \rangle = -\frac{4}{5}\epsilon r, \tag{1}$$

that can be derived from the three-dimensional NS equations under the assumption of high Reynolds number and flow isotropy [30–33]. Here, $\epsilon$ is the time-averaged dissipation rate, $r$ is the two-point displacement, and the coefficient -4/5 is a direct result of the NS equations. In terms of coefficients in turbulence scalings, also relevant is the recent work by de Silva et al. [34]. The authors matched velocity scalings at small and large scales and determined the constants in the velocity scalings of $\langle \Delta u^n \rangle$ for $r > z$.

This work aims to address the above-mentioned two weaknesses. We study the behavior of the third-order structure function. From a fundamental standpoint, the third-order structure is a useful statistical tool and have been used in the studies two-dimensional turbulence [35–37], turbulence with bidirectional energy transfer [38–40], and anisotropic sheared turbulence [41–43]. Hence, studying the third-order function would lead to better understandings of the boundary-layer turbulence. Also, because Eq. (1) is exact, matching to Eq. (1) will allow us to determine the constants in our expression of the third-order structure function in the logarithmic layer. The rest of the paper is organised as follows. We present the theory in section II followed by empirical evidence in section III. Concluding remarks are given in section IV.

## II. THEORY

In this section, we investigate the behavior of the third-order structure function via AEH and the NS equations.

### A. Attached eddy hypothesis

We derive the scaling of the third-order structure function from AEH. Per AEH, the flow in the logarithmic layer can be modeled as a collection of wall-attached eddies [2, 6], as sketched in figure 1 (a). The velocity

at a generic location in the flow field is modeled as a sum of the attached-eddy-induced velocity increments [13, 14, 44]

$$u(z) = \sum_{i=1}^{N_z} a_i, \quad w(z) = b_{N_z}, \qquad N_z = \int_z^{\delta} P(z)dz, \qquad P(z) \sim 1/z. \tag{2}$$

Here, $u(z)$ and $w(z)$ are the instantaneous stream and wall-normal velocity fluctuations at a distance $z$ from the wall in the logarithmic layer. $a_i$ and $b_i$ are the $\delta/2^i$-sized attached-eddy-induced streamwise and wall-normal velocity. Obviously, because both $a_i$ and $b_i$ are due to an eddy of size $\delta/2^i$, $a_i$ and $b_i$ are correlated. That is, $\langle a_i a_i \rangle \sim \langle b_i b_i \rangle \sim \langle a_i b_i \rangle \neq 0$. Figure 1 (b) sketches how one can go about computing the attached eddy induced velocity. The streamwise velocity results from an additive process that adds up contributions from attached eddies whose heights are larger than $z$. The wall-normal velocity contains the contribution from the attached eddy of size $z$ only. $N_z$ is the number of wall-attached eddies that contribute to $u(z)$. By definition, $N_z$ equals the integration of the eddy population density $P(z)$ from $z$, the height of the smallest wall-attached eddy that affects the velocity at the wall-normal height $z$, to $\delta$, the height of the largest wall-attached eddy in the flow. Because the sizes of the wall-attached eddies scale as their distances from the wall, the eddy population density $P(z)$ is proportional to $1/z$.

It follows from Eq. (2) that the third-order moments in the logarithmic layer is:

$$\left\langle u^3 \right\rangle = \left\langle \left( \sum_{i=1}^{N_z} a_i \right)^3 \right\rangle = \sum_{i=1}^{N_z} \left\langle a_i^3 \right\rangle \sim N_z \left\langle a^3 \right\rangle \sim \ln(\delta/z). \tag{3}$$

Here, the cross terms $\langle a_i a_j a_k \rangle = 0$, for $i \neq j \neq k$, and $\left\langle a_i a_j^2 \right\rangle = 0$ for $i \neq j$ because differently-sized eddies are not statistically correlated; $a_i$'s are statistically similar and $\left\langle a_i^3 \right\rangle = \left\langle a^3 \right\rangle$. Single-point logarithmic scalings like the one in Eq. (3) have two-point counterparts. For example, the single-point logarithmic scaling in $\left\langle u^2 \right\rangle \sim \ln(\delta/z)$ has the two-point counterpart $\left\langle (u(x+r) - u(x))^2 \right\rangle \sim \ln(r/z)$ [34]. While the $\left\langle (u(x+r) - u(x))^3 \right\rangle \sim \ln(r/z)$ does exist, its derivation will be slightly different from its second order counterpart.

Given two points that are displaced by a distance $r$ in the streamwise direction, we have

$$u(x,z) = \sum_{i=1}^{N_z} a_i, \quad u(x+r,z) = \sum_{i=1}^{N_z} a_i' \tag{4}$$

where $a_i$'s are velocity increments that contribute to $(x,z)$ and $a_i'$'s are velocity increments that contribute to $(x+r,z)$. It follows from Eq. (4) that the velocity difference is

$$u(x,z) - u(x+r,z) = \sum_{i=1}^{N_z} (a_i - a_i'). \tag{5}$$

A large-scale attached eddy (colored yellow in figure 1 a) contributes the same increment to both $(x,z)$ and $(x+r,z)$, and a small-scale attached eddy (colored red in figure 1 a) contributes to neither $(x,z)$ nor $(x+r,z)$. Hence, $u(x,z) - u(x+r,z)$ contains contributions from intermediate-sized eddies only:

$$u(x,z) - u(x+r,z) = \sum_{i=N_r}^{N_z} (a_i - a_i'), \quad N_r \sim \ln(\delta/r). \tag{6}$$

Squaring both sides of Eq. (6) and taking ensemble average, we have the logarithmic scaling of the second order structure function

$$\begin{aligned} \left\langle [u(x,z) - u(x+r,z)]^2 \right\rangle &\sim (N_z - N_r)(\left\langle a_i^2 \right\rangle + \left\langle a_i'^2 \right\rangle - 2 \left\langle a_i a_i' \right\rangle) \\ \sim (N_z - N_r)(\left\langle a^2 \right\rangle - \left\langle a a' \right\rangle) &\sim (N_z - N_r) \sim \ln(r/z) = D_2 \log(r/z) + B_2, \end{aligned} \tag{7}$$

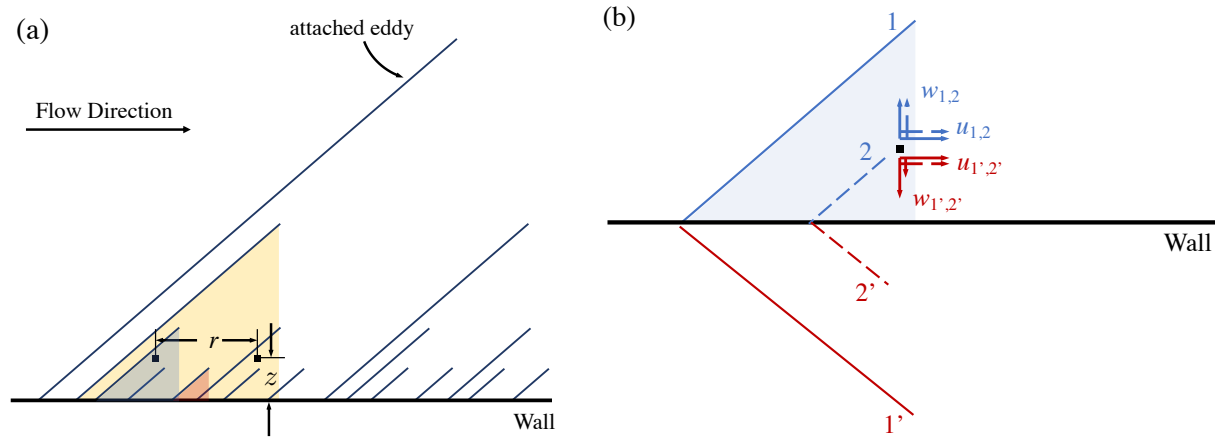


FIG. 1. (a) A schematic of the attached eddies. An attached eddy is represented as an inclined line. The two points are at a distance $z$ from the wall and are displaced by a distance $r$ in the streamwise direction. (b) Computing the induced velocity of an attached eddy at a location in the flow field. The induced velocity is modeled by adding up the induced velocities from eddies 1, 2 and 1', 2'. Here, eddy 1' is the mirror of eddy 1, and eddy 2' is the mirror of eddy 2. $w_{1,2}$ and $w_{1',2'}$ are the wall-normal velocities induced by eddies 1, 2 and 1', 2', and $u_{1,2}$ and $u_{1',2'}$ are the streamwise velocities induced by eddies 1, 2 and eddy 1', 2'. For a large eddy, here eddy 1, $w_1$ is approximately balanced by its mirror $w_{1'}$, and the wall-normal velocity at $z$ is determined by the local wall-attached eddy only, for which $w_2$ is much larger than $w_{2'}$.

where $D_2$ and $B_2$ are two constants. The two constants are usually thought to be independent of $z$, and $D_2$ is usually considered to be universal [17, 34, 45]. Here, $\langle a_i a_j' \rangle = 0$ for $i \neq j$, $\langle a_i a_j \rangle = \langle a_i' a_j' \rangle = 0$ for $i \neq j$ because differently sized eddies are statistically uncorrelated; $a$ and $a'$ are statistically similar to $a_i$ and $a_i'$. We can get an estimate of the third-order structure function following the same steps. Raising both sides of Eq. (6) to the third power and taking ensemble average, we have

$$\begin{aligned} &\langle [u(x,z) - u(x+r,z)]^3 \rangle \sim (N_z - N_r) \left( \langle a_i a_i'^2 \rangle - \langle a_i' a_i^2 \rangle \right) \\ &\sim (N_z - N_r) \left( \langle a a'^2 \rangle - \langle a' a^2 \rangle \right) \sim N_z - N_r \sim \ln(r/z) = D_3 \ln(r/z) + B_3. \end{aligned} \tag{8}$$

Again, differently sized eddies are not statistically correlated. The two terms $\langle a a'^2 \rangle$ and $\langle a' a^2 \rangle$ do not cancel because correlation in one direction is different from that in another direction. (In fact, in isotropic turbulence, we have $\langle a a'^2 \rangle = -\langle a' a^2 \rangle$ due to symmetry.) The exact value of the two terms depend on the exact topology of an attached eddy and therefore is left undetermined in the present framework. AEH itself gives only the scaling but not the constants $D_3$ and $B_3$. Following previous studies [34, 46], the constant $D_3$ is expected to be universal, and the constant $B_3$ is expected to be flow dependent. Following the same steps, one can also get a logarithmic scaling for the third-order structure function of the spanwise velocity $\langle \Delta v^3 \rangle \sim \ln(r/z)$, whose behavior will not be the focus of this work. The complex anisotropic nature of the flow cannot be fully captured by the streamwise velocity's streamwise structure function. However, measuring velocity correlations for $r_y \neq 0$ and $r_z \neq 0$ is not as straight-forward as measuring velocity correlations for $r_y = r_z = 0$ in an experiment, the latter requires one-point hot-wire measurements whereas the former requires simultaneous measurements at two points for various two-point displacements. Considering a lack of validation data for more general statistics and given the purpose of this work, we would study $\langle \Delta u^3(r_x) \rangle$ only.

In anticipation of the discussion in section II B, we discuss a few implications of AEH. First, the wall-normal velocity is solely determined by the local wall-attached eddy (see figure 1b and Ref [2] for a detailed discussion). Second, at a wall normal height $z$, the number of attached eddies that contribute to $\Delta u_i$ is proportional to $\ln(r/z)$ (see figure 1a and Ref [47] for detailed discussion), and therefore any statistics that comprises of $\Delta u_i$ is a function of $r/z$ only. It follows that $d(u_i(x,z) - u_i(x+r, z+r_z))/dr_z|_{r_z=0} = 0$ and

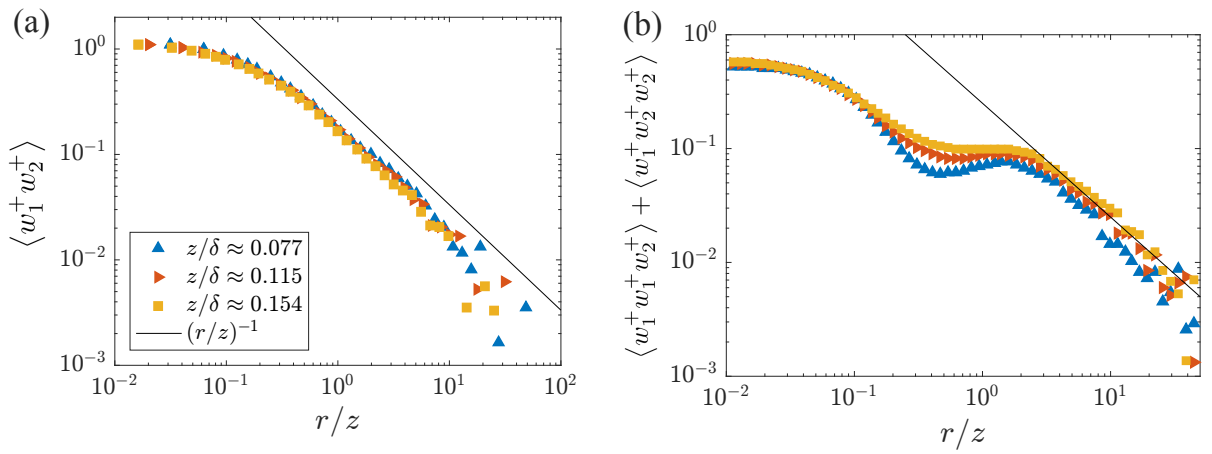


FIG. 2. (a) Auto-correlation of the wall-normal velocity in a $Re_\tau = 5200$ channel [16]. The subscript 1 and 2 denote the two points. (b) Same as (a) but for $\langle w_1^+ w_2^+ w_2^+ \rangle + \langle w_1^+ w_1^+ w_2^+ \rangle$.

$d(u_i(x,y,z) - u_i(x+r, y+r_y, z))/dr_y|_{r_y=0} = 0$ because slightly displacing either point in the wall-normal or the spanwise direction does not change the number of wall-attached eddies that contribute to the velocity difference $\Delta u_i$. In fact, following the discussion in Refs. [9, 47], if given a streamwise distance $r_x$, the spanwise and the wall normal displacements make a difference only when $r_y > r_x AR_y$ and $r_z > r_x AR_z$, where $AR_y$ and $AR_z$ are the aspect ratio of a wall-attached eddy. We note that the discussion here concerns the scales that are relevant to the logarithmic layer only. These derivatives, $\partial/\partial r_y$, $\partial/\partial r_z$, are 0 under the basic assumptions of AEH and for $r_y/z \ll 1$ and $r_z/z \ll 1$. These derivatives are not necessarily 0 at other scales [48]. In fact, the term $\partial \langle |\Delta u|^2 \Delta w \rangle / \partial r_z$ equals $2d \langle kw \rangle / dz$ and is certainly non-zero ($\langle kw \rangle$ only depend on $z$ hence the total derivative). Here, by arguing that they are 0, we are arguing that the attached eddies, i.e., the large scales, do not contribute to these terms. In this particular case here, the term $d \langle kw \rangle / dz$ and the pressure-strain term are negligible as the dissipation and the production balance in the logarithmic layer [16]. Also, one can plot $\langle kw \rangle$'s and $\langle wp/\rho \rangle$'s spectra to confirm/repute the AEH's conclusion, where $k$ is the turbulent kinetic energy and $p$ is the pressure fluctuation. Lee & Moser [49] reported these spectra in channel, and we see that both $\langle kw \rangle$ and $\langle wp/\rho \rangle$ are small and large scale contributions to these two terms are also small. Last, for some statistics that involves the wall-normal velocity, e.g., $\langle w_1 w_2 \rangle$, AEH only gives estimate for sufficiently large $r/z$. The behavior of $\langle w_1 w_2 \rangle$ for $r/z \approx 1$ cannot be known unless one specifies the geometry of the attached eddies. Nevertheless, the behavior of $\langle w_1 w_2 \rangle$ for intermediate $r/z$ (e.g., $r/z = 2$, 3) should not depend on the exact geometry of the attached eddies and can be obtained from the Biot-Savart law [7, 50, 51]. To elaborate, as $w(x,z)$ is solely determined by the attached eddy at $(x,z)$, the correlation between $w(x,z)$ and the velocity at any location in the flow field is solely determined by the eddy at $(x,z)$. For sufficiently large $r/z$, AEH predicts $\langle w(x,z)w(x+r,z) \rangle = 0$. For intermediate $r$, the Biot-Savart law gives $\langle w(x,z)w(x+r,z) \rangle \sim 1/(r/z)$. A more detailed discussion of the application of the Biot-Savart law could be found in Ref [7]. The authors found that the intensity of an attached eddy decays as a function of $\sim 1/r(r^2+\text{const})$. Taking the leading order term directly leads to $1/r$. Figure 2 (a) shows $\langle w(x,z)w(x+r,z) \rangle$ as a function of $r/z$ in a channel flow at the Reynolds number $Re_\tau = 5200$, and a $-1$ scaling is indeed found. Similarly, AEH predicts $\langle w(x,z)u(x+r,z) \rangle = 0$, $\langle w(x,z)u(x,z)u(x+r,z) \rangle = 0$ for sufficiently large $r/z$, but for intermediate $r/z$, $\langle w(x,z)u(x+r,z) \rangle \sim \langle w(x,z)w(x+r,z) \rangle \sim 1/(r/z)$, $\langle u(x,z)u(x+r,z)w(x+r,z) \rangle \sim \langle w(x,z)w(x+r,z)w(x+r,z) \rangle \sim 1/(r/z)$—as correlations among these velocity fluctuations are due to the same attached eddy at $(x,z)$. Figure 2 (b) shows $\langle w(x,z)w(x+r,z)w(x+r,z) \rangle + \langle w(x,z)w(x,z)w(x+r,z) \rangle$ as a function of $r/z$, and, a $-1$ scaling is also found at $r/z$ values that are relevant to the logarithmic range.

### B. Navier-Stokes equations

We evaluate the terms in the Kármán-Howarth-Monin (KHM) equation according to AEH and show that the remaining terms in the NS equations give rise to consistent results. Writing the transport equation for the second-order structure function in a fully developed plane channel and time averaging [52], we have

$$\begin{aligned}&\frac{\partial\left\langle|\Delta\mathbf{u}|^2\Delta u_i\right\rangle}{\partial r_i}+2\left\langle\Delta u\Delta w\right\rangle\frac{dU}{dz}+\frac{\partial\left\langle w_c|\Delta\mathbf{u}|^2\right\rangle}{\partial z_c}\\=&-4\left\langle\epsilon\right\rangle+2\nu\frac{\partial^2\left\langle|\Delta\mathbf{u}|^2\right\rangle}{\partial r_i\partial r_i}-\frac{2}{\rho}\frac{\partial\left\langle\Delta p\Delta w\right\rangle}{\partial z_c}+\frac{\nu}{2}\frac{\partial^2\left\langle|\Delta\mathbf{u}|^2\right\rangle}{\partial z_c^2}.\end{aligned}\tag{9}$$

Here, $\mathbf{u}=(u,v,w)$ is the instantaneous velocity fluctuation vector. $v$ and $w$ are the instantaneous spanwise and wall-normal velocity fluctuations. $U$ is the mean streamwise velocity profile. $x$, $y$, and $z$ are the streamwise, spanwise, and wall-normal directions. $\Delta$ denotes the difference between two points that are displaced by $\boldsymbol{r}=(r_x,r_y,r_z)$ direction, e.g., $\Delta u=u(\boldsymbol{x}+\boldsymbol{r})-u(\boldsymbol{x})=u_2-u_1$ with the subscripts 1 and 2 denote point 1 at $\boldsymbol{x}_1=\boldsymbol{x}$ and point 2 at $\boldsymbol{x}_2=\boldsymbol{x}+\boldsymbol{r}$. $w_c=(w_1+w_2)/2$, $z_c=(z_1+z_2)/2$, and we will later set $z_c=z_1=z_2=z$ as we consider horizontal displacement only. $\epsilon$ is the dissipation rate, $\nu$ is the kinematic viscosity. $r_i$ is the displacement between the two points in the three Cartesian directions. $\rho\equiv1$ is the fluid density. $p$ is the pressure.

Before we examine the various terms in Eq. (9), we briefly review the literature on pressure fluctuations in the logarithmic layer. In an early paper [53], Jiménez and Hoyas examined channel flow DNS at $Re_\tau=2000$ and argued that pressure and spanwise velocity fluctuations have similar behaviors. In the past decade, higher Reynolds number data become available, and these data have led to new insights. In two recent works [54, 55], the authors examined data at higher Reynolds numbers and came to the conclusion that spanwise velocity fluctuations are large scale quantities and pressure fluctuations are small scale quantities. Specifically, at sufficiently high Reynolds numbers, velocity fluctuations in the logarithmic layer are dominated by the scales near the so-called "outer" peak (note that an outer peak exists in both the spanwise and the streamwise velocities' premultiplied spectra), and pressure fluctuations are dominated by the scales near the inner peak. Hence, correlation between velocity and pressure should be small at sufficiently high Reynolds numbers. Now, we examine Eq. (9). For $r/z<1$, the flow is approximately isotropic, and Eq. (9) reduces to the KHM equation (see section II C 1 for more details). For $r/z$ and $z$ values that are relevant to the logarithmic layer, the viscous terms are negligible, the pressure/velocity correlation is close to 0 because of the scale separation at high Reynolds numbers [54, 55], and the production balances the dissipation [1, 2]

$$\epsilon\approx-\left\langle uw\right\rangle\frac{dU}{dz}=\frac{u_\tau^3}{\kappa z},\tag{10}$$

where $-\left\langle uw\right\rangle=u_\tau^2$ in the constant-stress layer (logarithmic layer), $U=1/\kappa\ln(z^+)+B$ is assumed with $B\approx5.0$, and $\kappa$ is the von Kármán constant. Hence, for $r/z$ and $z$ in the logarithmic layer, Eq. (9) becomes

$$\frac{\partial\left\langle|\Delta\mathbf{u}|^2\Delta u_i\right\rangle}{\partial r_i}+\frac{\partial\left\langle w_c|\Delta\mathbf{u}|^2\right\rangle}{\partial z}=2\left\langle u_1w_2+w_1u_2\right\rangle\frac{u_\tau}{\kappa z}.\tag{11}$$

Per AEH, $\left\langle\Delta u^2\Delta u_i\right\rangle$, $\left\langle w_c\Delta u^2\right\rangle$, and $\left\langle u_1w_2+w_1u_2\right\rangle$ are only function of $r_h/z$ with $r_h=\sqrt{r_x^2+r_y^2}$ (see the

discussion in section II A). Defining $r'_x = r_x/z$, $r'_y = r_y/z$, $r'_z = r_z$, $z' = z$, and $r'_h = \sqrt{r'^2_x + r'^2_y}$, we have

$$\begin{aligned}
\frac{\partial}{\partial r_x} &= \frac{\partial}{\partial r'_x}\frac{\partial r'_x}{\partial r_x} + \frac{\partial}{\partial r'_y}\frac{\cancel{\partial r'_y}}{\cancel{\partial r_x}} + \frac{\partial}{\partial r'_z}\frac{\cancel{\partial r'_z}}{\cancel{\partial r_x}} + \frac{\partial}{\partial z'}\frac{\cancel{\partial z'}}{\cancel{\partial r_x}} = \frac{1}{z}\frac{\partial}{\partial r'_x} \\
\frac{\partial}{\partial z} &= \frac{\partial}{\partial r'_x}\frac{\partial r'_x}{\partial z} + \frac{\partial}{\partial r'_y}\frac{\partial r'_y}{\partial z} + \frac{\partial}{\partial r'_z}\frac{\cancel{\partial r'_z}}{\partial z} + \frac{\cancel{\partial}}{\cancel{\partial z'}}\frac{\partial z'}{\partial z} = -\frac{r'_x}{z}\frac{\partial}{\partial r'_x} - \frac{\cancel{r'_y}}{\cancel{z}}\frac{\partial}{\partial r'_y} \\
\frac{\partial}{\partial r'_h} &= \frac{\partial}{\partial r'_x}\frac{\partial r'_x}{\partial r'_h} + \frac{\partial}{\partial r'_y}\frac{\partial r'_y}{\partial r'_h} + \frac{\partial}{\partial r'_z}\frac{\cancel{\partial r'_z}}{\cancel{\partial r'_h}} + \frac{\partial}{\partial z'}\frac{\cancel{\partial z'}}{\cancel{\partial r'_h}} \\
&= \cos(\theta)\frac{\partial}{\partial r'_x} + \cancel{\sin(\theta)}\frac{\partial}{\partial r'_y} = \frac{r'_x}{r}\frac{\partial}{\partial r'_x}.
\end{aligned} \tag{12}$$

Here, we have invoked $r_y = r'_y = 0$, $\partial/\partial r_z = 0$, $\partial/\partial r_y = 0$, and $\partial/\partial z' = 0$. Again, these derivatives are 0 under the basic assumptions of AEH and for $r_y/z \ll 1$ and $r_z/z \ll 1$. The angle $\theta$ is such that $r'\cos(\theta) = r'_x$, $r'\sin(\theta) = r'_y$. It follows that Eq. (11) becomes

$$\frac{\partial\left\langle|\Delta\mathbf{u}|^2\Delta u\right\rangle}{\partial r'_x} - r'_x\frac{\partial\left\langle|\Delta\mathbf{u}|^2 w_c\right\rangle}{\partial r'_x} = 2\left\langle u_1 w_2 + w_1 u_2\right\rangle\frac{u_\tau}{\kappa}. \tag{13}$$

Observe that the $z'$ dependence is removed from Eq. (13). For sufficiently large $r', r'_x$, all the terms in Eq. (13) are 0 and the equation is trivial. For intermediate $r', r'_x$,

$$\left\langle u_1 w_2 + w_1 u_2\right\rangle \sim \frac{1}{r'_x}, \quad \left\langle|\Delta\mathbf{u}|^2 w_c\right\rangle \sim \frac{1}{r'_x}, \tag{14}$$

following the discussion in the previous subsection. Again, the question we hope to answer here is: what would these velocity correlations be under the basic assumption of AEH? While there are different theories in the existing literature that give rise to somewhat different scaling estimates [56, 57], and studying the effect of these scalings would be an interesting topic, here, we would focus on Townsend's attached eddy hypothesis and refrain from invoking scaling estimates that are not consequences of AEH. Substituting Eq. (14) into Eq. (13), we have

$$\frac{\partial\left\langle|\Delta\mathbf{u}|^2\Delta u\right\rangle}{\partial r'_x} \sim \frac{1}{r'_x}, \tag{15}$$

which in turn gives rise to

$$\left\langle|\Delta\mathbf{u}|^2\Delta u\right\rangle \sim \ln(r/z) + C, \tag{16}$$

where $C$ is a constant. Computing $\left\langle|\Delta\mathbf{u}|^2\Delta u\right\rangle$ requires simultaneous measurement of the streamwise, spanwise, and wall-normal velocity components, which is usually not trivial in a laboratory experiment. If $\left\langle\Delta u^3\right\rangle \gg \left\langle\Delta v^2\Delta u\right\rangle, \left\langle\Delta w^2\Delta u\right\rangle$, Eq. (16) reduces to Eq. (8). We will discuss this issue in section III in greater detail.

### C. Asymptotic matching

Next, we determine the two constants $D_3$ and $B_3$ in Eq. (8) via asymptotic matching. We show that our procedure connects the constants in small-scale velocity scalings and large-scale (logarithmic-layer) velocity scalings.

#### 1. *Kolmogorov's theory of small scale turbulence*

According to Kolmogorov [58], in three-dimensional homogeneous and isotropic turbulence, the viscous scale and the integral scale do not play an important role in the inertial sub-range, and the velocity structure

function is a function of $r$ and $\epsilon$ only, that is

$$\langle \Delta u^n \rangle = C_n (\epsilon r)^{n/3}, \tag{17}$$

where $\Delta u$ is the longitudinal velocity difference of two points with a distance $r$, $n$ is an integer, and $C_n$ is a universal constant. Specifically, the third-order structure function

$$\langle \Delta u^3 \rangle = C_3 \epsilon r, \quad C_3 = -4/5, \tag{18}$$

is a direct result of Eq. (9) [31]. It is worth noting that if $r$ is only in the $x$ direction, we have

$$\begin{aligned} \frac{\partial \langle \Delta u^3 \rangle}{\partial r_y} &= \frac{d \langle \Delta u^3 \rangle}{dr} \frac{\partial r}{\partial r_y} = \frac{d \langle \Delta u^3 \rangle}{dr} \frac{2 r_y}{r} = 0, \\ \frac{\partial \langle \Delta u^3 \rangle}{\partial r_z} &= \frac{d \langle \Delta u^3 \rangle}{dr} \frac{\partial r}{\partial r_z} = \frac{d \langle \Delta u^3 \rangle}{dr} \frac{2 r_z}{r} = 0, \end{aligned} \tag{19}$$

as well. Hence, $\partial/\partial r_y = \partial/\partial r_z = 0$ is not a consequence of AEH but a consequence of limiting the displacement in one of the three Cartesian directions. In addition to the third-order structure function, the second-order structure function is

$$\langle \Delta u^2 \rangle = C_2 (\epsilon r)^{2/3}, \quad C_2 \approx 2.0. \tag{20}$$

Sreenivasan [59] concluded from pipe, channel, grid turbulence, wake turbulence, mixing layer, and jet data that the Kolmogorov constant $C_2 = 4C_K \approx 2.0$ is universal at high Taylor micro Reynolds numbers, i.e., $Re_\lambda > 50$, where $C_K \approx 0.5$ is the Kolmogorov constant in the $-5/3$ energy spectral law. The universality of $C_n$ for $n$ other than 2 and 3 has received much less attention. A naive estimation of $C_n$ can be obtained by assuming Gaussianality for $\Delta u^2$:

$$C_{2n} = C_2[(2n-1)!!], \tag{21}$$

where $(2n-1)!! = (2n-1)(2n-3)\cdots 1$. This, of course, is only a very rough approximation of the reality.

### 2. *Matching Townsend's attached eddy hypothesis and Kolmogorov's theory of small scale turbulence*

The small-scale velocity scalings hold in boundary-layer flows for $r/z < 1$ [34, 60–62], and these small-scale velocity scalings connect to Townsend's scalings of energy-containing momentum-transferring scales without much of a transitional region. For example, the energy spectrum follows the $-5/3$ scaling for $1/z < k$ and the $-1$ scaling for $k < 1/z$ [61, 62]. de Silva et al. [34] reported $\langle \Delta u^2 \rangle = C_2 (\epsilon r)^{2/3}$, i.e., small-scale velocity scaling, for $r/z < 1$ and the logarithmic scaling of the streamwise velocity variance, i.e., Townsend's scaling, for $r/z > 1$, in a $Re_\tau = 13,000$ boundary layer. To determine $B_3$ and $D_3$, we match AEH's scalings and Kolmogorov's velocity scalings.

Define

$$r' = r/z. \tag{22}$$

Equations (18) and (8) give

$$\begin{aligned} \langle \Delta u^3 \rangle &= C_3' r', \\ \langle \Delta u^3 \rangle &= B_3 + D_3 \ln(r'), \end{aligned} \tag{23}$$

where $C_3' = C_3 \epsilon z / u_\tau^3$. Again, the dissipation rate $\epsilon$ balances the production and $\epsilon \approx -\langle uw \rangle (dU/dz) = u_\tau^3/(\kappa z)$ [1, 2]. Taylor expanding the two expressions in Eq. (23) at $r_0$ where Eq. (18) and Eq. (8) match, we have

$$\langle \Delta u^{+3} \rangle = C_3' r_0 + C_3' dr', \tag{24a}$$

$$\langle \Delta u^{+3} \rangle = B_3 + D_3 \ln(r_0) + D_3 \frac{dr'}{r_0} + \text{h.o.t.}, \tag{24b}$$

where h.o.t. denotes higher order terms. Matching the leading order term in the two expressions in Eq. (24), we have

$$C_3' = \frac{1}{r_0} D_3. \tag{25}$$

Because Eq. (18) and Eq. (8) match at $r/z = 1$, i.e., $r_0 = 1$, Eq. (25) leads to

$$D_3 = C_3' = \frac{1}{\kappa} C_3. \tag{26}$$

Taking $\kappa = 0.4$ we obtain that $D_3 = C_3' = -2$, which we later justify using experimental and numerical data. Up to this point, we have obtained an estimate of $\langle \Delta u^3 \rangle$ for $r$ and $z$ that are relevant to the logarithmic layer without explicitly referring to empirical evidence.

Although it is not the focus of this work, the above procedure may well be used to get the constants in the second order structure function, i.e., $D_2$ and $B_2$ in

$$\langle \Delta u^2 \rangle = D_2 \ln(r/z) + B_2. \tag{27}$$

Again, define

$$r' = (r/z)^{2/3}. \tag{28}$$

It follows from Eq. (20) and Eq. (27) that

$$\langle \Delta u^{+2} \rangle = C_2' r', \tag{29a}$$

$$\langle \Delta u^{+2} \rangle = B_2 + \frac{3}{2} D_2 \ln(r'), \tag{29b}$$

where $C_2' = C_2 (\epsilon z)^{2/3} / u_\tau^2$. Taylor expanding at $r_0$ and matching the leading order term in the two expressions in Eq. (29), we have

$$C_2' = \frac{3}{2 r_0} D_2. \tag{30}$$

Again, $r_0 = 1$, and Eq. (30) gives

$$D_2 = \frac{2}{3} \frac{(\epsilon z)^{2/3}}{u_\tau^2} C_2 = \frac{2}{3} \kappa^{-2/3} C_2. \tag{31}$$

In the above expression, taking the von Kármán constant as $\kappa = 0.4$ and the Kolmogorov constant as $C_2 = 2$, we obtain that $D_2 \approx 2.5$. Because $D_2$ equals two times the Townsend-Perry constant, the above estimate leads to an estimate of the Townsend-Perry constant $A_2 = 1.25$, which is consistent with experimental and numerical evidence [45].

Following roughly the same steps, we can also get

$$D_{2n} = \frac{2}{3} \kappa^{-2/3} C_{2n}^{1/n}. \tag{32}$$

If one invokes Eq. (21), Eq. (32) gives

$$D_{2n} = D_2 [(2n-1)!!]^{1/n}, \tag{33}$$

i.e., the estimates in Ref [46]. This shows that the Gaussianality of velocity statistics in the logarithmic layer, or the non-Gaussianality of the velocity statistics in the logarithmic layer for that matter, is a direct consequence of the Gaussianality of the velocity statistics in the inertial range.

TABLE I. Details of the dataset. Here $\Delta y^+$ for experiments refers to the hot wire filtration.

| Figure | Facility | Reference | Technique | $\approx Re_\tau$ | $\approx \Delta x^+$ | $\approx \Delta y^+$ | $\approx \Delta z^+$ |
|---|---|---|---|---|---|---|---|
| Figure 3(a) | Melbourne | [65] | Hotwire | 13,000 | — | 20 | — |
| Figure 3(c) | Melbourne | [68] | PIV | 19,000 | 15 | 30 | 15 |
| Figure 3(b) | — | [16] | DNS | 5,200 | 12.7 | 6.4 | $0.5 \sim 10.3$ |
| Figure 3(d) | SLTEST | [67] | Hotwire | $3 \times 10^6$ | — | 15 | — |

## III. EMPIRICAL EVIDENCE

Empirical evidence for many of the velocity statistics has already been reported. For example, de Silva et al. [34] presented empirical evidence for the velocity scalings in Eq. (20) and Eq. (27) in boundary-layer flows as well as the transition from Eq. (20) to Eq. (27) at $r/z = 1$. Here, we present empirical evidence for the logarithmic scaling of the third-order structure function, i.e., Eq. (8).

To this end, four databases are used to cover several decades of Reynolds number and two canonical boundary layer flow geometries with the key parameters summarised in table I. We note databases that have friction Reynolds numbers that exceed $Re_\tau \gtrsim 5000$ or higher are chosen in the present analysis such that the flow can be considered to be at high Reynolds numbers [63], where there is sufficient scale separation to decouple the viscous and energetic scales [64], and over a decade of logarithmic velocity variation in $z^+$.

Two datasets are acquired from the High Reynolds Number Boundary Layer Wind Tunnel (HRNBLWT) at the University of Melbourne. The wind tunnel has a test section of 27 m, which provides a high Reynolds number at low flow speeds with a large viscous scale that leads to less acute spatial resolution issues. The hotwire database from this facility is acquired using a 2.5$\mu$m diameter Wollasten wires operated by an in-house constant-temperature anemometer (MUCTA) with sufficient spatial resolution to resolve the turbulence intensity accurately within the log-region [65]. The second database from the same facility is obtained using two-dimensional two-component Particle Image Velocimetry (PIV) measurements. These measurements utilise a multi-camera arrangement to capture both a large field-of-view (FOV) in the order of $\delta$ and a highly magnified FOV. For the present analysis we utilise the high magnification view which has sufficient spatial resolution to resolve spatial scales of the order of $\eta$. Moreover, the PIV measurements provide direct spatial information hence we do not need to invoke Taylor's Frozen Hypothesis to compute structure functions which is necessary for all the hotwire datasets.

A direct numerical data is also utilised from a channel flow geometry with a friction Reynolds number $Re_\tau = 5200$ [16]. For this database, the computation domain is $8\pi \times 2 \times 3\pi$ in the streamwise ($x$), wall-normal ($y$), and spanwise ($z$) directions, respectively. The half channel height is unity (=1). The dataset was generated and maintained by the University of Texas at Austin, and the raw field data can be accessed through the Johns Hopkins Turbulence Database [66].

The final dataset is captured using hot-wire anemometry at the Surface Layer Turbulence and Environmental Test facility (SLTEST) located in the Utah salt flats [67]. The measurements involved a vertical array of 2.5 $\mu$m diameter platinum-coated tungsten wires mounted from $z = (0.005 - 2)$ m, which are predominantly located in the logarithmic region of the flow. The database is valuable for this analysis as it provides a significantly higher friction Reynolds number of $\mathcal{O}(10^6)$.

Figure 3 (a) shows $\langle \Delta u^3 \rangle$ as a function of $r/z$ in the $Re_\tau = 13000$ boundary layer at $z^+ \approx 400$, 700, 1000. Figure 3 (b) shows $\langle \Delta u^3 \rangle$ in the $Re_\tau = 5200$ channel at $z^+ \approx 400$, 600, 800. Figure 3 (c, d) shows the PIV data and the SLTEST data. We note, the PIV data is limited in terms of its $r$ range and the SLTEST atmospheric boundary layer data is somewhat affected by its statistical convergence (Getting statistically converged data at the neutral condition in the atmosphere is challenging), and is also affected by the uncertainty in estimating the friction velocity (see [34]). Nevertheless, comparing the PIV data in (c) and the hotwire data in (a), we see that the Taylor's hypothesis does not seem to have an impact on the statistics. Comparing the SLTEST data in (d) and the PIV data in (c), we see that the logarithmic scaling of the third-order structure function is persistent at high Reynolds numbers. In the following, we focus on

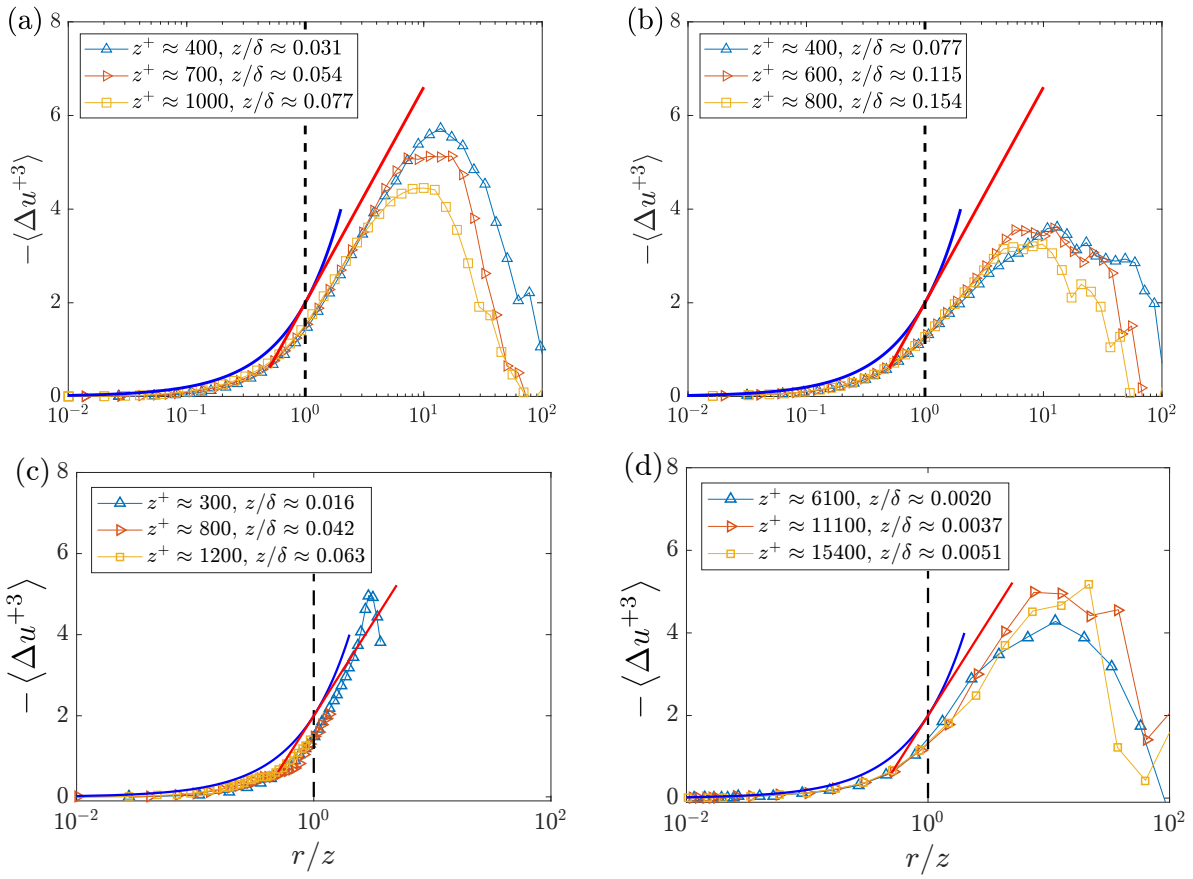


FIG. 3. Third-order longitudinal structure functions in (a) a turbulent boundary layer at $Re_\tau \approx 13000$ at $z^+ = 400$, 700, 1000, (b) a turbulent channel at $Re_\tau \approx 5200$ at $z^+ = 400$, 600, 800, (c) a turbulent boundary layer at $Re_\tau \approx 19000$ at $z^+ = 300$, 800, 1200 and (d) the atmospheric boundary layer at $Re_\tau \approx 3 \times 10^6$ at $z^+ \approx 6100$, 11100, 15400. The blue solid lines correspond to $C_3 = 4/5$. The red solid lines correspond to $D_3 = 2.0$. The von Kármán constant $\kappa$ is set to 0.40 here.

the results in (a, b), where we have statistically converged data at several heights and across a (relatively) large $r$ range. The data follows Eq. (18) for $r/z < 1$ and exhibit a logarithmic behavior as indicated in Eq. (8) between $1 < r/z \lesssim 10$. The high Reynolds number of the boundary layer in (a) pushes the data towards the prediction with $C_3 = -4/5$ and $D_3 = -2.0$, but there is still a notable difference between the prediction of the KHM equation and the data, suggesting local anisotropy at even the Reynolds number of $Re_\tau = 13000$. Last, figure 4 compares $\langle |\Delta \mathbf{u}|^2 \Delta u \rangle$ and $\langle \Delta u^3 \rangle$ in a channel. For $r/z \sim O(1)$, the streamwise component does dominate and $\langle |\Delta \mathbf{u}|^2 \Delta u \rangle \approx \langle \Delta u^3 \rangle$.

## IV. CONCLUSIONS

AEH suffers from two weaknesses. First, AEH does not predict the constants in log-layer velocity scalings; and second, AEH's predictions cannot be obtained from the NS equations. These two weaknesses separate AEH from more credible theories like Kolmogorov's theory of small-scale turbulence. This work attempts to address the above two weaknesses by investigating the behavior of the third-order structure function in the logarithmic layer. First, we show that both AEH and the NS equations lead to a logarithmic scaling of the third-order structure function: $\langle \Delta u^3 \rangle = D_3 \ln(r/z) + B_3$. Second, we determine the constant $D_3$ via asymptotic matching. Specifically, the matching procedure relates the universal constants in boundary-layer

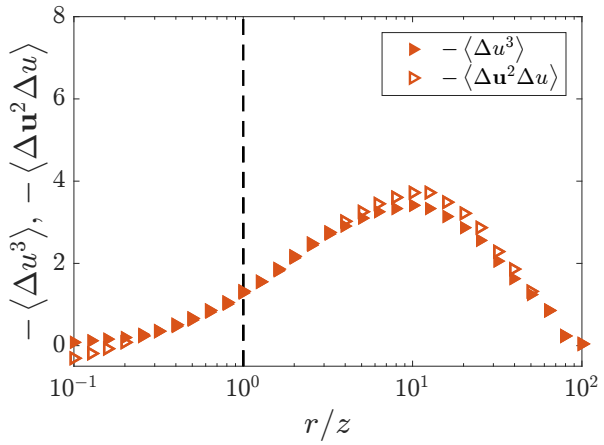


FIG. 4. $-\langle\Delta u^3\rangle$ and $-\langle|\Delta\mathbf{u}|^2\Delta u\rangle$ at $z/\delta = 0.11$ in a $Re_\tau = 5200$ channel.

velocity scalings to the constants in Kolmogorov's phenomenology of small-scale turbulence, and it gives $D_3 = -2$. In addition to $D_3$, we show that our matching procedure gives an estimate to the Townsend-Perry constant, i.e., $A_1 = 1.25$, which is very close to the existing measurements.

Last, we note that even at the Reynolds number $Re_\tau = 13000$, the third-order structure function deviates from the exact relation $\langle\Delta u^3\rangle = -4/5\epsilon r = -4/5\left(u_\tau^3/\kappa\right)(r/z)$ for small $r$, suggesting either an imbalance between the production and the dissipation or flow anisotropy at small scales, both of which are usually considered to be finite Reynolds number effects. Hence, for this problem and a number of other problems in the recent literature [69, 70], there is still a need for high-quality high Reynolds number flow data.

## ACKNOWLEDGEMENT

J-HX gratefully acknowledges financial support from the National Natural Science foundation of China grant No. 92052102. XY is supported by the US Office of Naval Research under contract N000142012315, with Dr. Peter Chang as Technical Monitor. RH acknowledges the financial supports from NSFC No. 11972175. CDS thanks the ARC for financial support.

[1] H. Tennekes and J. L. Lumley, *A first course in turbulence*. MIT Press, 1972.
[2] A. Townsend, *The structure of turbulent shear flow*. Cambridge University Press, 1976.
[3] J. Jiménez, "Cascades in wall-bounded turbulence," *Annu. Rev. Fluid Mech.*, vol. 44, pp. 27–45, 2012.
[4] T. Wei, "Integral properties of turbulent-kinetic-energy production and dissipation in turbulent wall-bounded flows," *J. Fluid Mech.*, vol. 854, pp. 449–473, 2018.
[5] A. J. Smits, B. J. McKeon, and I. Marusic, "High-Reynolds number wall turbulence," *Annu. Rev. Fluid Mech.*, vol. 43, pp. 353–375, 2011.
[6] I. Marusic and J. P. Monty, "Attached eddy model of wall turbulence," *Annu. Rev. Fluid Mech.*, vol. 51, pp. 49–74, 2019.
[7] A. E. Perry and M. S. Chong, "On the mechanism of wall turbulence," *J. Fluid Mech.*, vol. 119, pp. 173–217, 1982.
[8] I. Marusic, "On the role of large-scale structures in wall turbulence," *Phys. Fluids*, vol. 13, no. 3, pp. 735–743, 2001.
[9] C. M. De Silva, J. D. Woodcock, N. Hutchins, and I. Marusic, "Influence of spatial exclusion on the statistical behavior of attached eddies," *Phys. Rev. Fluids*, vol. 1, no. 2, p. 022401, 2016.

[10] W. J. Baars, N. Hutchins, and I. Marusic, "Self-similarity of wall-attached turbulence in boundary layers," *J. Fluid Mech.*, vol. 823, p. R2, 2017.

[11] R. Baidya, J. Philip, N. Hutchins, J. Monty, and I. Marusic, "Distance-from-the-wall scaling of turbulent motions in wall-bounded flows," *Phys. Fluids*, vol. 29, no. 2, p. 020712, 2017.

[12] J. D. Woodcock and I. Marusic, "The statistical behaviour of attached eddies," *Phys. Fluids*, vol. 27, no. 1, p. 015104, 2015.

[13] X. I. A. Yang, I. Marusic, and C. Meneveau, "Hierarchical random additive process and logarithmic scaling of generalized high order, two-point correlations in turbulent boundary layer flow," *Phys. Rev. Fluids*, vol. 1, no. 2, p. 024402, 2016.

[14] X. I. A. Yang and C. Meneveau, "Hierarchical random additive model for wall-bounded flows at high Reynolds numbers," *Fluid Dyn. Res.*, vol. 51, no. 1, p. 011405, 2019.

[15] R. Hu, X. I. A. Yang, and X. Zheng, "Wall-attached and wall-detached eddies in wall-bounded turbulent flows," *J. Fluid Mech.*, vol. 885, p. A30, 2020.

[16] M. K. Lee and R. D. Moser, "Direct numerical simulation of turbulent channel flow up to $Re_\tau \approx 5200$," *J. Fluid Mech.*, vol. 774, pp. 395–415, 2015.

[17] M. Hultmark, M. Vallikivi, S. C. C. Bailey, and A. J. Smits, "Turbulent pipe flow at extreme Reynolds numbers," *Phys. Rev. Lett.*, vol. 108, no. 9, p. 094501, 2012.

[18] P. A. Davidson, T. B. Nickels, and P.-Å. Krogstad, "The logarithmic structure function law in wall-layer turbulence," *J. Fluid Mech.*, vol. 550, pp. 51–60, 2006.

[19] P. A. Davidson, P.-Å. Krogstad, and T. B. Nickels, "A refined interpretation of the logarithmic structure function law in wall layer turbulence," *Phys. Fluids*, vol. 18, no. 6, p. 065112, 2006.

[20] J. Klewicki, P. Fife, and T. Wei, "On the logarithmic mean profile," *J. Fluid Mech.*, vol. 638, p. 73, 2009.

[21] J. C. Klewicki, "Self-similar mean dynamics in turbulent wall flows," *J. Fluid Mech.*, vol. 718, pp. 596–621, 2013.

[22] J. C. Del Álamo and J. Jiménez, "Linear energy amplification in turbulent channels," *J. Fluid Mech.*, vol. 559, pp. 205–213, 2006.

[23] A. S. Sharma and B. J. McKeon, "On coherent structure in wall turbulence," *J. Fluid Mech.*, vol. 728, pp. 196–238, 2013.

[24] R. Moarref, A. S. Sharma, J. A. Tropp, and B. J. McKeon, "Model-based scaling of the streamwise energy density in high-Reynolds-number turbulent channels," *J. Fluid Mech.*, vol. 734, pp. 275–316, 2013.

[25] B. J. McKeon, "The engine behind (wall) turbulence: perspectives on scale interactions," *J. Fluid Mech.*, vol. 817, p. P1, 2017.

[26] B. J. McKeon, "Self-similar hierarchies and attached eddies," *Phys. Rev. Fluids*, vol. 4, no. 8, p. 082601, 2019.

[27] Y. Hwang and B. Eckhardt, "Attached eddy model revisited using a minimal quasi-linear approximation," *J. Fluid Mech.*, vol. 894, p. A23, 2018.

[28] A. Lozano-Durán and H. J. Bae, "Characteristic scales of townsend's wall attached eddies," *arXiv preprint arXiv:1901.04613*, 2019.

[29] C. Cheng, W. Li, A. Lozano-Durán, and H. Liu, "Uncovering townsend's wall-attached eddies in low-reynolds-number wall turbulence," *J. Fluid Mech.*, vol. 889, p. A29, 2020.

[30] T. von Kármán and L. Howarth, "On the statistical theory of isotropic turbulence," *Proc. Math. Phys. Eng. Sci.*, vol. 164, no. 917, pp. 192–215, 1938.

[31] A. N. Kolmogorov, "Dissipation of energy in the locally isotropic turbulence," in *Dokl. Akad. Nauk SSSR A*, vol. 32, pp. 16–18, 1941.

[32] A. S. Monin and A. M. Yaglom, *Statistical fluid mechanics, volume II: Mechanics of turbulence*. Dover (reprinted 2007), 1975.

[33] U. Frisch, *Turbulence: the legacy of A. N. Kolmogorov*. Cambridge university press, 1995.

[34] C. M. De Silva, I. Marusic, J. D. Woodcock, and C. Meneveau, "Scaling of second-and higher-order structure functions in turbulent boundary layers," *J. Fluid Mech.*, vol. 769, pp. 654–686, 2015.

[35] E. Lindborg, "Can the atmospheric kinetic energy spectrum be explained by two-dimensional turbulence?," *J. Fluid Mech.*, vol. 388, pp. 259–288, 1999.

[36] D. Bernard, "Three-point velocity correlation functions in two-dimensional forced turbulence," *Phys. Rev. E*, vol. 60, no. 5, pp. 6184–6187, 1999.

[37] V. Yakhot, "Two-dimensional turbulence in the inverse cascade range," *Phys. Rev. E*, vol. 60, no. 5, pp. 5544–5551, 1999.

[38] A. Alexakis and L. Biferale, "Cascades and transitions in turbulent flows," *Phys. Rep*, vol. 767–769, pp. 1–101, 2018.

[39] J.-H. Xie and O. Bühler, "Two-dimensional isotropic inertia–gravity wave turbulence," *J. Fluid. Mech.*, vol. 872, pp. 752–783, 2019.

[40] J.-H. Xie and O. Bühler, "Third-order structure functions for isotropic turbulence with bidirectional energy transfer," *J. Fluid Mech.*, vol. 877, p. R3, 2019.

[41] C. M. Casciola, P. Gualtieri, R. Benzi, and R. Piva, "Scale-by-scale budget and similarity laws for shear turbulence," *J. Fluid. Mech.*, vol. 476, pp. 105–114, 2003.

[42] M. Wan, S. Servidio, S. Oughton, and W. H. Matthaeus, "The third-order law for increments in magnetohydrodynamic turbulence with constant shear," *Phys. Plasmas*, vol. 16, p. 090703, 2009.

[43] M. Wan, S. Servidio, S. Oughton, and W. H. Matthaeus, "The third-order law for magnetohydrodynamic turbulence with shear: Numerical investigation," *Phys. Plasmas*, vol. 17, p. 052307, 2010.

[44] X. I. A. Yang, R. Baidya, Y. Lv, and I. Marusic, "Hierarchical random additive model for the spanwise and wall-normal velocities in wall-bounded flows at high Reynolds numbers," *Phys. Rev. Fluids*, vol. 3, no. 12, p. 124606, 2018.

[45] I. Marusic, J. P. Monty, M. Hultmark, and A. J. Smits, "On the logarithmic region in wall turbulence," *J. Fluid Mech.*, vol. 716, p. R3, 2013.

[46] C. Meneveau and I. Marusic, "Generalized logarithmic law for high-order moments in turbulent boundary layers," *J. Fluid Mech.*, vol. 719, p. R1, 2013.

[47] X. I. A. Yang, R. Baidya, P. Johnson, I. Marusic, and C. Meneveau, "Structure function tensor scaling in the logarithmic region derived from the attached eddy model of wall-bounded turbulent flows," *Phys. Rev. Fluids*, vol. 2, no. 6, p. 064602, 2017.

[48] D. Gatti, A. Chiarini, A. Cimarelli, and M. Quadrio, "Structure function tensor equations in inhomogeneous turbulence," *J. Fluid Mech.*, vol. 898, 2020.

[49] M. K. Lee and R. D. Moser, "Spectral analysis of the budget equation in turbulent channel flows at high Reynolds number," *J. Fluid Mech.*, vol. 860, pp. 886–938, 2019.

[50] A. E. Perry and I. Marusic, "A wall-wake model for the turbulence structure of boundary layers. Part 1. extension of the attached eddy hypothesis," *J. Fluid Mech.*, vol. 298, pp. 361–388, 1995.

[51] I. Marusic and A. E. Perry, "A wall-wake model for the turbulence structure of boundary layers. Part 2. further experimental support," *J. Fluid Mech.*, vol. 298, pp. 389–407, 1995.

[52] A. Cimarelli, E. De Angelis, and C. Casciola, "Paths of energy in turbulent channel flows," *J. Fluid Mech.*, vol. 715, pp. 436–451, 2013.

[53] J. Jiménez and S. Hoyas, "Turbulent fluctuations above the buffer layer of wall-bounded flows," *J. Fluid Mech.*, vol. 611, pp. 215–236, 2008.

[54] Y. Tsuji, I. Marusic, and A. V. Johansson, "Amplitude modulation of pressure in turbulent boundary layer," *Int. J. Heat Fluid Flow*, vol. 61, pp. 2–11, 2016.

[55] H. H. A. Xu, A. Towne, X. I. A. Yang, and I. Marusic, "Pressure power spectrum in high-Reynolds number wall-bounded flows," *Int. J. Heat Fluid Flow*, vol. 84, p. 108620, 2020.

[56] J. Lumley, "Interpretation of time spectra measured in high-intensity shear flows," *The physics of fluids*, vol. 8, no. 6, pp. 1056–1062, 1965.

[57] B. Jacob, C. M. Casciola, A. Talamelli, and P. H. Alfredsson, "Scaling of mixed structure functions in turbulent boundary layers," *Phys. Fluids*, vol. 20, no. 4, p. 045101, 2008.

[58] A. N. Kolmogorov, "The local structure of turbulence in incompressible viscous fluid for very large Reynolds numbers," *C.R. Acad. Sci. U.R.S.S.*, vol. 30, pp. 301–305, 1941.

[59] K. R. Sreenivasan, "On the universality of the Kolmogorov constant," *Phys. Fluids*, vol. 7, no. 11, pp. 2778–2784, 1995.

[60] S. G. Saddoughi and S. V. Veeravalli, "Local isotropy in turbulent boundary layers at high Reynolds number," *J. Fluid Mech.*, vol. 268, pp. 333–372, 1994.

[61] T. B. Nickels, I. Marusic, S. Hafez, and M. S. Chong, "Evidence of the $k_1^{-1}$ law in a high-reynolds-number turbulent boundary layer," *Phys. Rev. Lett.*, vol. 95, no. 7, p. 074501, 2005.

[62] X. I. A. Yang, S. Pirozzoli, and M. Abkar, "Scaling of velocity fluctuations in statistically unstable boundary-layer flows," *J. Fluid Mech.*, vol. 886, 2020.

[63] A. Smits, B. McKeon, and I. Marusic, "High-Reynolds number wall turbulence," *Ann. Rev. Fluid Mech.*, vol. 43, pp. 353 – 75, 2011.

[64] B. J. McKeon and J. F. Morrison, "Asymptotic scaling in turbulent pipe flow," *Phil. Trans. Royal Soc. A: Math., Phys. Eng. Sci.*, vol. 365, no. 1852, pp. 771–787, 2007.

[65] N. Hutchins, T. B. Nickels, I. Marusic, and M. S. Chong, "Hot-wire spatial resolution issues in wall-bounded turbulence," *J Fluid Mech*, vol. 635, pp. 103–136, 2009.

[66] J. Graham, K. Kanov, X. I. A. Yang, M. Lee, N. Malaya, C. C. Lalescu, R. Burns, G. Eyink, A. Szalay, R. D. Moser, and C. Meneveau, "A web services accessible database of turbulent channel flow and its use for testing a new integral wall model for LES," *J. Turbul.*, vol. 17, no. 2, pp. 181–215, 2016.

[67] G. J. Kunkel and I. Marusic, "Study of the near-wall-turbulent region of the high-Reynolds number boundary layer using an atmospheric flow," *J. Fluid Mech.*, vol. 548, pp. 375–402, 2006.

[68] C. M. de Silva, E. Gnanamanickam, C. Atkinson, N. A. Buchmann, N. Hutchins, J. Soria, and I. Marusic, "High spatial range velocity measurements in a high reynolds number turbulent boundary layer," *Phys. Fluids*, vol. 26, no. 2, p. 025117, 2014.

[69] X. Chen, F. Hussain, and Z.-S. She, "Non-universal scaling transition of momentum cascade in wall turbulence," *J. Fluid Mech.*, vol. 871, 2019.

[70] X. Chen and K. R. Sreenivasan, "Reynolds number scaling of the peak turbulence intensity in wall flows," *J. Fluid Mech.*, vol. 908, 2021.